The role of PKC and PKD in CXCL12 and CXCL13 directed malignant melanoma and acute monocytic leukemic cancer cell migration

Isabel Hamshaw, Youssef Ellahouny, Artur Malusickis, Lia Newman, Dante Ortiz-Jacobs, Anja Mueller [*]

School of Pharmacy, University of East Anglia, Norwich NR4 7TJ, UK

ABSTRACT

Cancer metastasis is the leading cause of cancer related mortality. Chemokine receptors and proteins in their downstream signalling axis represent desirable therapeutic targets for the prevention of metastasis. Despite this, current therapeutics have experienced limited success in clinical trials due to a lack of insight into the downstream signalling pathway of specific chemokine receptor cascades in different tumours. In this study, we investigated the role of protein kinase C (PKC) and protein kinase D (PKD) in CXCL12 and CXCL13 stimulated SK-MEL-28 (malignant melanoma) and THP-1 (acute monocytic leukaemia) cell migration. While PKC and PKD had no active role in CXCL12 or CXCL13 stimulated THP-1 cell migration, PKC and PKD inhibition reduced CXCL12 stimulated migration and caused profound effects upon the cytoskeleton of SK-MEL-28 cells. Furthermore, only PKC and not PKD inhibition reduced CXCL13 stimulated migration in SK-MEL-28 cells however PKC inhibition failed to stimulate any changes to the actin cytoskeleton. These findings indicate that PKC inhibitors would be a useful therapeutic for the prevention of both CXCL12 and CXCL13 stimulated migration and PKD inhibitors for CXCL12 stimulated migration in malignant melanoma.

1. Introduction

66–90% of cancer related deaths are due to metastasis [1,2]. In accordance with Paget's seed and soil hypothesis, metastatic patterns are related to specific cancer tumour cell types (seeds) preferentially migrating to certain organs (soil) [3]. Chemokines and chemokine receptors have long been implicated as a factor in this organ-specific 'seed and soil' metastatic process [4,5]. Chemokines are low molecular weight proteins (8–30 kDa) that stimulate directed cell migration along a concentration gradient [6]. Specifically, the binding of the chemokine to its corresponding chemokine receptor on the cancer cell leads to conformational change, which activates downstream signalling pathways that promote migration [7]. Therefore, chemokine receptors and their downstream signalling axis, represent desirable therapeutic targets for the prevention of metastasis.

The binding of both CXCL12 to CXCR4 and CXCL13 to CXCR5 mediates the activation of receptor associated heterotrimeric G protein. Briefly, the $G_{\alpha q}$ subunit activates phospholipase C β (PLCβ) which hydrolyses the conversion of phosphatidylinositol 4, 5-bisphosphateto inositol triphosphate (IP3) and diacylglycerol (DAG). Both IP3 and DAG can either directly activate PKC or can indirectly activate PKC through the release of Ca^{2+}. Additionally, the Gβγ dimer can also activate PLCβ and IP3 thus leading to PKC activation [8–11].

PKCs are a family of serine/threonine kinases consisting of 11 isoforms, classified according to their activation requirements [12]. The classical (also known as conventional) PKC isoforms; α, βI, βII, and γ are dependent upon both DAG and Ca^{2+} for activation while novel PKC isoforms; δ, ε, η, and θ require only DAG for activation. Finally, the atypical PKC isoforms; ζ and λ/ι are not directly activated via the PLCβ pathway therefore, they do not require DAG or Ca^{2+} for activation [9,13]. Instead, they are activated via secondary messages downstream of DAG or by alternative downstream pathways such as through Src protein and phosphoinositide 3-kinase activation [8,14].

Similarly, the PKD family of serine/threonine kinases consists of three isoforms; PKD1, PKD2 and PKD3. Activation of PKDs occurs via several biological agents including DAG in a similar pathway to PKCs as well as by PKC itself or through oxidative stress via tyrosine residue phosphorylation [15,16].

PKC and PKD can have both promotive and suppressive effects upon tumour growth and metastasis dependent upon the cancer cell type and the specific isoform that has been activated [17–24]. This highlights the importance of determining the role of different PKC and PKD isoforms in different cancer cell types when activated by chemokine receptor pathways.

In this study we focus upon two distinct cell types: SK-MEL-28 malignant melanoma cells and THP-1 acute monocytic leukaemia cells derived from a patient with acute monocytic leukaemia (AML-M5; AMoL), a subtype of acute myeloid leukaemia (AML) [25,26]. Using specific PKC and PKD inhibitors, we investigate the role of these proteins in both CXCR4 and CXCR5 directed leukaemia and melanoma cell migration.

2. Results

2.1. SK-MEL-28 and THP-1 cells have different CXC receptor expression profiles

Prior to detailed studies of CXC receptor migration, the receptor profiles of the malignant melanoma cell line, SK-MEL-28, and the AML-M5 cell line, THP-1, were characterised. This determined that the SK-MEL-28 cells had significant expression of both CXCR4 and CXCR5 chemokine receptors (Fig. 1A, Table 1) which was validated through immunofluorescence imaging (Fig. 1B-D). Alternatively, THP-1 cells had significant expression of CXCR2, CXCR3 and CXCR4 (Fig. 1E, Table 1). The effect of CXCR1, CXCR2 and CXCR3 in CXCL8 and CXCL10 directed migration in THP-1 cells has previously been investigated by our group [27].Therefore, while relative expression of CXCR5 in THP-1 cells was not as high in comparison to CXCR1 (4.22 ± 1.93), CXCR2 (26.81 ± 7.23) and CXCR3 (23.34 ± 3.81), there was still sufficient expression of CXCR5 (4.00 ± 1.30) for investigation. Expression of CXCR4 and CXCR5 in THP-1 cells was also validated by immunofluorescence imaging (Fig. 1F-H).

2.2. CXCL12 and CXCL13 induced migration in SK-MEL-28 cells is inhibited by PKC inhibitors but not by PKD inhibitors

Maximum tolerated concentrations of five PKC and PKD inhibitors were examined in both SK-MEL-28 and THP-1 cells to determine the highest tolerated concentration range for each inhibitor (Table 2). Following this, we sought to investigate the effect of PKC and PKD inhibitors on CXCL12 and CXCL13 induced SK-MEL-28 migration using time-lapse microscopy that has successfully been utilised for cell migratory studies in other adherent cell lines including prostate and breast cancer [27,28]. 5 half log incremental concentrations of PKC or PKD inhibitor within the tolerated toxicity range (GF109203X; 300 nM to 30 μM, staurosporine; 1 nM to 100 nM, ZIP; 300 nM to 10 μM, CID2011756; 300 nM to 30 μM and CID755673; 300 nM to 30 μM) in the presence of 10 nM CXCL12 or CXCL13 were added to the SK-MEL-28 cells. The PKC inhibitors GF109203X, ZIP and staurosporine evoked a dose dependent decrease in both CXCL12 and CXCL13 chemokine stimulated migration (Fig. 2 and Tables 3-4). Alternatively, only the maximum concentration of PKD inhibitors (30 μM of both CID2011756 and CID755673) inhibited CXCL12 and CXCL13 induced SK-MEL-28 migration. At this concentration CID2011756 and CID755673 not only inhibits PKD1–3 but can also weakly inhibit PKC, therefore the inhibition seen is unlikely to be due to PKD inhibition [29]. Of the five tested PKC and PKD inhibitors, staurosporine was the most potent (pIC$_{50}$ 8.99 $\pm$ 0.57 (1.02 nM) in the presence of CXCL12 and pIC$_{50}$ 7.90 $\pm$ 0.51 (12.58 nM) in the presence of CXCL13) followed by ZIP (pIC$_{50}$ 6.61 $\pm$ 0.68 (0.24 μM) in the presence of CXCL12 and pIC$_{50}$ 5.98 $\pm$ 0.66 (1.05 μM) in the presence of CXCL13) then GF109203X (pIC$_{50}$ 5.30 $\pm$ 0.43 (5.02 μM) in the presence of CXCL12 and pIC$_{50}$ 5.56 $\pm$ 0.42 (2.78 μM) in the presence of CXCL13). In general, the PKC and PKD inhibitors had higher potency when inhibiting CXCL12 induced migration over CXCL13 induced migration.
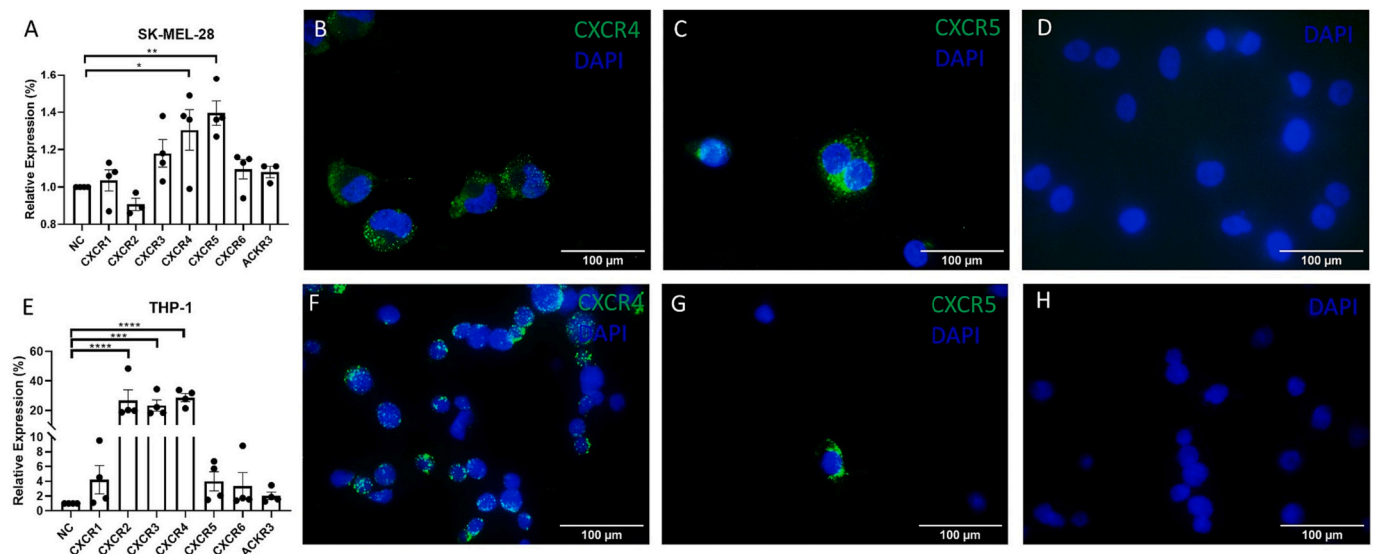

Fig. 1. CXC receptor expression in malignant melanoma (SK-MEL-28) and acute monocytic leukemic (THP-1) cell lines. A) Relative CXC receptor expression profile of SK-MEL-28 cells. B) CXCR4 and C) CXCR5 verses D) negative control in SK-MEL-28 cells. E) Relative CXC receptor expression profile of THP-1 cells. F) CXCR4 and G) CXCR5 verses H) negative control in THP-1 cell. Relative CXC receptor expression calculated as median fluorescence intensity of sample/median fluorescence intensity of negative control (cells incubated with anti-mouse Alexa Fluor® 488). Values acquired using CytExpert v2.4 (Beckman Coulter). Absolute values are shown in Table 2. CXC receptors visualised using primary mouse anti-CXCR4 (12G5) or primary mouse anti-CXCR5 (MU5UBEE) and secondary anti-mouse Alexa Fluor® 488 with nuclei indicated by DAPI staining. Negative control visualised using anti-mouse Alexa Fluor® 488 and DAPI staining only. Data shows representative cells from 4 independent experiments with similar findings. Acquired with Leica imaging suite, 63× objective (35× overall magnification). Data are mean $\pm$ SEM, *N* = 4. One-Way ANOVA and post hoc Dunnett's multiple comparison test comparing expression to negative control (NC), *$p < 0.05$, **$p < 0.01$, **$p < 0.001$ and ****$p < 0.0001$. Outliers identified using Grubb's alpha = 0.05.

Table 1

Relative chemokine receptor expression in SK-MEL-28 and THP-1 cell lines.

Cell line	CXCR1	CXCR2	CXCR3	CXCR4	CXCR5	CXCR6	ACKR3
THP-1	4.22 ± 1.93	26.81 ± 7.23 ****	23.34 ± 3.81 ***	28.73 ± 2.76 ****	4.00 ± 1.30	3.37 ± 1.82	2.04 ± 0.49
SKMEL-28	1.04 ± 0.06	0.91 ± 0.03	1.18 ± 0.07	1.31 ± 0.11 *	1.40 ± 0.07 *	1.10 ± 0.05	1.08 ± 0.03

Relative expression calculated as median fluorescence intensity (MFI) of sample/ MFI of negative control. Data are mean ± SEM, $N = 4$ independent experiments (data were analysed by one-way ANOVA and Dunnett's multiple comparison test comparing receptor expression to negative control *$p < 0.05$, **$p < 0.01$, ***$p < 0.001$ and ****$p < 0.0001$.

Table 2

PKC and PKD inhibitors do not cause toxicity in SK-MEL-28 or THP-1 cells lines.

Inhibitor	Concentrations	SK-MEL-28	THP-1
GF109203X	300 nM - 30 μM	Non-toxic	Non-toxic
PKCζ	100 nM - 10 μM	Non-toxic	Non-toxic
CID2011756	300 nM - 30 μM	Non-toxic	Non-toxic
CID755673	300 nM - 30 μM	Non-toxic	Non-toxic
Staurosporine	1 nM – 100 nM	Non-toxic	Non-toxic

One-Way ANOVA and post hoc Dunnett's multiple comparison test comparing positive control to incremental half log concentrations of PKC and PKD inhibitors. Data representative of 3 independent experiments.

2.3. CXCL12 and CXCL13 induced migration in THP-1 cells is not inhibited by PKC or PKD inhibitors

Maximum tolerated concentrations of the PKC or PKD inhibitors were used to investigate the effect of PKC and PKD inhibitors on CXCL12 and CXCL13 induced THP-1 cell migration. Due to the lack of adhesion required for leukemic cancer cells, time lapse microscopy is not a suitable method of analysis. However, chemotaxis plates that have successfully been utilised for cell migratory studies in suspension cell lines including both THP-1 and Jurkat cells, were use for this study [27,30] (Fig. 3). Neither the PKC nor the PKD inhibitors had any significant effect upon THP-1 cell migration.

2.4. PKC inhibitors prevent CXCL12 stimulated SK-MEL-28 cellular morphological changes

To determine if the PKC or PKD inhibitors instigated an effect upon the cytoskeleton of SK-MEL-28 cells, immunofluorescence analysis was conducted using the maximum tolerated concentrations of each inhibitor. It was determined that the addition of 10 nM CXCL12 induced a significant increase in SK-MEL-28 cell surface area while 10 nM CXCL13 induced a significant decrease in SK-MEL-28 cell surface area (Figs. 4 and 5) All three PKC inhibitors (GF109203X, ZIP and staurosporine) significantly reduced CXCL12 stimulated SK-MEL-28 cell surface area however, there was no significance as compared to 10 nM CXCL13. The two PKD inhibitors (CID2011756 and CID755673) did not have any significant effect upon SK-MEL-28 cell surface area.

Regarding cell circularity, SK-MEL-28 cells have a very elongated cell morphology that was not significantly changed by the addition of chemokine however, there was an overall trend that the addition of 10 nM CXCL12 decreased SK-MEL-28 circularity (i.e., the cells become more elongated) and 10 nM CXCL13 increased circularity. It was observed that the addition of GF109203X and CID2011756 significantly increased SK-MEL-28 circularity as well as a trend that ZIP, staurosporine and CID755673 increased the circularity of CXCL12 stimulated SK-MEL-28 cells. There was no overall effect or trend of PKC or PKD inhibition upon CXCL13 induced circularity.
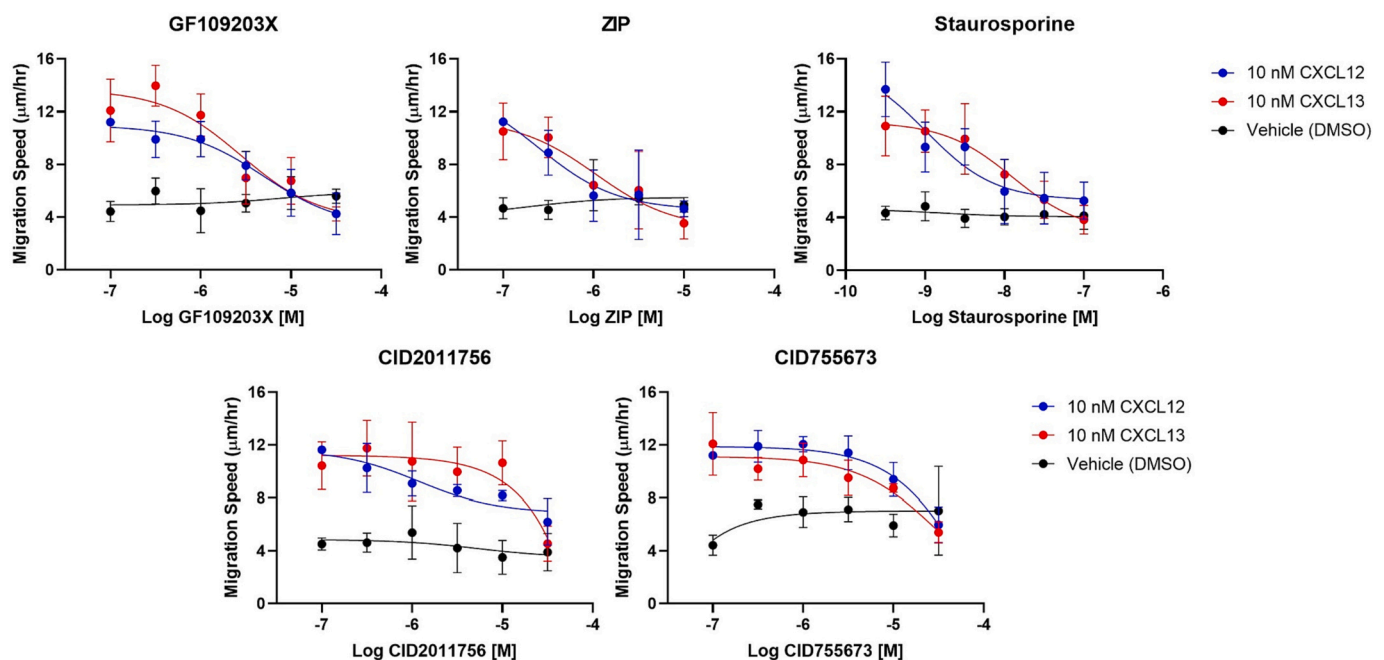

Fig. 2. Effect of PKC and PKD inhibitors upon CXCL12/CXCL13 stimulated SKMEL28 cell migration. PKC/PKD inhibitor +10 nM CXCL12 (blue) or 10 nM CXCL13 (red) or DMSO vehicle equivalent (black) concentration–response curves. All IC$_{50}$ and pIC$_{50}$ values obtained are shown in Table 3. Data are means ± SEM, $N = 4$ analysed by one-way ANOVA and post hoc Dunnett's multiple comparison test comparing PKC/PKD inhibitor treatment to 10 nM CXCL12 or CXCL13. Statistical values shown in Table 4. (For interpretation of the references to colour in this figure legend, the reader is referred to the web version of this article.)

Table 3
Summary statistics of PKC/PKD inhibitors upon CXCL12/CXCL13 stimulated SK-MEL-28 cell migration.

All inhibitors in the presence of 10 nM CXCL12					
Parameters	0.3–30 μM GF109203X	0.3–10 μM ZIP	1 nM – 1 μM Staurosporine	0.3–30 μM CID2011756	0.3–30 μM CID755673
IC_{50}	5.02 μM	0.24 μM	1.02 nM	1.18 μM	89.93 μM
$pIC_{50} \pm$ SEM	5.30 ± 0.43	6.61 ± 0.68	8.99 ± 0.57	5.93 ± 0.56	4.05 ± 1.38

All inhibitors in the presence of 10 nM CXCL13					
Parameters	0.3–30 μM GF109203X	0.3–10 μM ZIP	1 nM – 1 μM Staurosporine	0.3–30 μM CID2011756	0.3–30 μM CID755673
IC_{50}	2.78 μM	1.05 μM	12.58 nM	n/a	30.58 μM
$pIC_{50} \pm$ SEM	5.56 ± 0.42	5.98 ± 0.66	7.90 ± 0.51	n/a	4.52 ± 0.86

Equation = Log (Inhibitor) vs. response – Variable slope (four parameters) Hill Slope = 1. Data representative of the mean SEM ± of 4 independent experiments.

Table 4
Statistical significance of PKC/PKD inhibitors upon CXCL12/CXCL13 stimulated SK-MEL-28 cell migration as depicted in Fig. 2.

10 nM CXCL12					
Concentration	GF109203X	Staurosporine	ZIP	CID2011756	CID755673
1 nM	n/a	ns 0.3409	n/a	n/a	n/a
3 nM	n/a	ns 0.3440	n/a	n/a	n/a
10 nM	n/a	* 0.0255	n/a	n/a	n/a
30 nM	n/a	* 0.0162	n/a	n/a	n/a
100 nM	n/a	* 0.0138	n/a	n/a	n/a
300 nM	ns 0.9437	n/a	ns 0.7146	ns 0.8703	ns 0.9932
1 μM	ns 0.9443	n/a	* 0.0203	ns 0.3789	ns 0.9803
3 μM	ns 0.2935	n/a	ns 0.1036	ns 0.2128	ns 0.9998
10 μM	* 0.0314	n/a	* 0.0276	ns 0.1361	ns 0.6613
30 μM	** 0.0043	n/a	n/a	** 0.0085	** 0.0091

10 nM CXCL13					
Concentration	GF109203X	Staurosporine	ZIP	CID2011756	CID755673
1 nM	n/a	ns 0.9997	n/a	n/a	n/a
3 nM	n/a	ns 0.9958	n/a	n/a	n/a
10 nM	n/a	ns 0.4540	n/a	n/a	n/a
30 nM	n/a	ns 0.1182	n/a	n/a	n/a
100 nM	n/a	* 0.0319	n/a	n/a	n/a
300 nM	ns 0.9146	n/a	ns 0.9997	ns 0.9916	ns 0.7779
1 μM	ns 0.9998	n/a	ns 0.3671	ns 0.9998	ns 0.9561
3 μM	ns 0.1551	n/a	ns 0.2903	ns 0.9997	ns 0.5217
10 μM	ns 0.1301	n/a	* 0.0475	ns 0.9999	ns 0.2774
30 μM	* 0.0133	n/a	n/a	ns 0.1575	** 0.0059

Data are mean ± SEM, $N = 4$ (data were analysed by one-way ANOVA and post hoc Dunnett's multiple comparison test comparing PKC/PKD inhibitor treatment to 10 nM CXCL12/CXCL13. ns, not significant, $*p < 0.05$ and $**p < 0.01$.

2.5. Experimental concentrations of CXCL12 and CXCL13 do not induce proliferation in SK-MEL-28 or THP-1 cells

Experimental concentrations (10 nM) of CXCL12 and CXCL13 were used in comparison to the cytostatic inhibitor lovastatin (10 μM), to investigate the effect of these chemokines upon SK-MEL-28 and THP-1 cell proliferation (Fig. 6). Neither chemokine had any significant effect upon proliferation at concentrations used.

3. Discussion

Overexpression of chemokine receptors is a contributing factor to cancer migration and the metastasis of a primary tumour to secondary sites thus, chemokine receptors and their downstream signalling axis represent desirable therapeutic targets as reviewed in Vilgelm and Richmond [31]. In this study we focused upon a melanoma cancer cell line (SK-MEL-28) and compare findings to a leukemic cell line (THP-1). Melanoma commonly metastasise to other areas of skin, subcutaneous tissue, lymph nodes, lung, brain, liver, bone and intestines [32]. Alternatively, in leukaemia, specifically AML, metastasises commonly develops throughout the bone marrow and can spread to the central nervous system, spleen, liver and skin [33]. While data differs depending upon the tumour group, it is thought that between 66.7 and 90% of cancer related deaths are due to metastasis [1,2].

High CXCR4 expression occurs in a multitude of different cancers including but not limited to skin, pancreatic, breast, prostate, colorectal, lung, brain, and haematological malignancies [7,34–43]. Several studies have demonstrated that CXCR4 accelerates cancer metastasis, invasion, growth, and therapeutic resistance and therefore can be used as a predictive biomarker for a poor prognosis [11,34,40,41,44]. Additionally, the CXCR5-CXCL13 signalling axis is also implicated in the growth and progression of several cancers including colon, leukaemia, lung, breast, and prostate cancer [45–49].Therefore, in this study, we wanted to determine the effects of the chemokines CXCL12 and CXCL13 and their cognate receptors, CXCR4 and CXCR5, respectively, upon SK-MEL-28 and THP-1 cellular migration. These chemokines were selected based upon the relative expression of CXC receptors on both cell types (Fig. 1, Table 1). Furthermore, we wanted to determine the role of the downstream proteins PKC and PKD in CXCL12 and CXCL13 mediated migration using small molecule inhibitors acting upon different PKC or
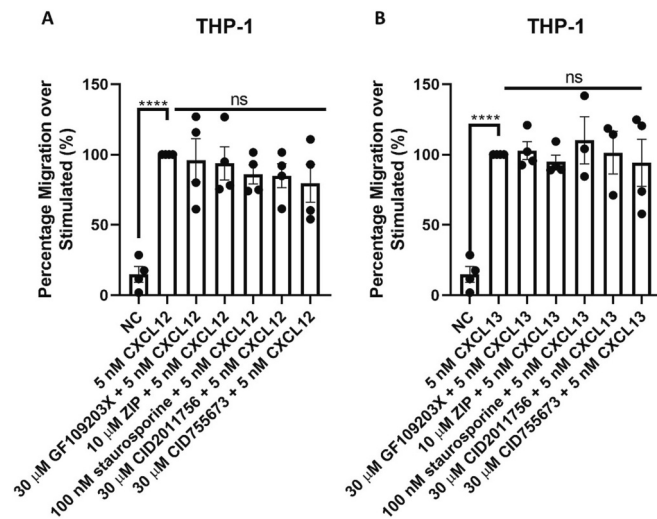
Fig. 3. Effect of PKC and PKD inhibitors upon CXCL12 and CXCL13 stimulated THP-1 cell migration. THP-1 cells were treated with 30 μM GF109203X, 10 μM ZIP, 100 nM staurosporine, 30 μM CID2011756 or 30 μM CID755673 and stimulated with either A) 5 nM CXCL12 or B) 5 nM CXCL13 for 4 h. Data are means ± SEM, $N = 4$ analysed by two-tailed, unpaired t-tests, comparing PKC/PKD inhibitor treatment to 5 nM CXCL12/CXCL13. Ns not significant and ****$p < 0.0001$.

PKD. It should be noted that while CXCL12 can also bind to ACKR3, expression levels in THP-1 and SK-MEL-28 cells lines were not significant however, it should be acknowledged that the results in this study may not reflect the response of CXCR4 only.

It has previously been reported that both PKC and PKD were important for the migration of CXCL12 stimulated metastatic prostate (PC3) cancer cells [28]. However, it was found that PKC inhibitors do not inhibit CCL3 induced migration in THP-1 cells [50]. Additionally, PKC inhibitors do not inhibit CXCL12 induced migration in acute T-cell leukaemia (Jurkat) cells however, they do inhibit CXCL12 stimulated migration in MCF-7 breast cancer cells [30]. Furthermore, PKCζ is important for the migration of CXCL10-stimulated PC3 cells, whereas it is not important for CXCL8-stimulated PC3 or MDA-MB-231 cells [27]. In this study we determined that both CXCL12 and CXCL13 increased SK-MEL-28 and THP-1 migration however, the effect of PKC and PKD inhibitors upon cellular migration and cellular morphology was variable dependent upon the cell line and the chemokine used.

Three PKC inhibitors GF109203X (α, βI, βII, γ, δ, ε and ζ PKC inhibitor), ZIP (PKCζ inhibitor) and staurosporine (α, γ, η, δ, ε and ζ PKC inhibitor) were employed and determined that PKC was crucial for both CXCL12 and CXCL13 induced SK-MEL-28 and THP-1 migration (Figs. 2 and 3). However, when using two non-specific PKD inhibitors; CID2011756 and CID755673, it was only at the highest concentration that inhibition was observed in CXCL12 stimulated SK-MEL-28 cells with only CID755673 causing inhibition in CXCL13 stimulated SK-MEL-28 cells. While it has not been confirmed if CID2011756 is capable of blocking PKC, >10 μM CID755673 has shown weak ability to block PKC. Therefore, PKD may be involved in CXCL12 stimulated SK-MEL-28 migration, but CXCL13 stimulated SK-MEL-28 migration is likely only to be driven by PKC and not PKD [29,51]. Opposing this, neither the PKC nor the PKD inhibitors any effect upon CXCL12 or CXCL13 stimulated migration in THP-1 cells (Fig. 3). This implicates that PKC and PKD are not required for CXCL12 nor CXCL13 stimulated migration in these cells.

Adherent cell migration as triggered by chemoattractants, stimulates cell morphological changes due to the reorganisation of the cellular actin cytoskeleton [52]. It is well known that PKC and PKD can trigger dynamic alterations in cellular morphology that lead to increased cellular adhesion thus increased migration [8,53–59]. Corroborating this, when stimulated with CXCL12 and CXCL13 there were distinct

changes upon the cellular morphology of SK-MEL-28 cells. Specifically, CXCL12 caused an increase in SK-MEL-28 cell surface area while the addition of GF109203X, ZIP and staurosporine decreased CXCL12 induced SK-MEL-28 cell surface area (Figs. 4 and 5). Regarding PKD, only CID2011756 demonstrated a trend of decreasing cell surface area while CID755673 had no observable effect upon CXCL12 induced SK-MEL-28 cell surface area. This indicates that PKC and PKD are involved in the reorganisation of the actin cytoskeleton of SK-MEL-28 cells when stimulated via CXCL12. Opposing this, CXCL13 caused a significant decrease in cell surface area with no observable changes to surface area with the addition of PKC or PKD inhibitors. To determine if the decrease in cell area was due to increased cell proliferation as stimulated by chemokine, MTS proliferation assays were employed in both SK-MEL-28 and THP-1 cells (Fig. 6). No significant differences were seen at experimental concentrations of chemokine suggesting that proliferation was not the cause of the cell area changes. It could be speculated that while both CXCL12 and CXCL13 enable melanoma cell migration, the different chemokines cause opposing effects upon cellular morphology depending upon the specific mode of cellular migration that they stimulate. Melanoma cells have been proven to use both mesenchymal and amoeboid-like modes of migration dependent upon their environment and it is possible that stimulation with different chemokines stimulate different modes of migration, hence differences in morphological shape [60]. For example, a transition of the SK-MEL-28 cells from mesenchymal to a more amoeboid-like migration, could explain why the addition of CXCL13 increased SK-MEL-28 migration while decreasing cell area and why THP-1 cells, which migrate via amoeboid migration, were not affected by PKC and PKD inhibitors [61–64]. However, to confirm this, further investigation would be required.

Overall, both the research presented here as well as previous work by this group has demonstrated that PKC and PKD have insubstantial involvement in chemokine stimulated leukemic cancer migration, likely due to the limited role of focal adhesions in suspension-based cancers [8,30,53–59]. Therefore, regarding therapeutics, PKC and PKD inhibition is unlikely to have beneficial results in preventing the metastasis of blood-based cancers. However, in solid tumours such as melanoma the benefit of PKC and PKD inhibition would depend upon the chemokines that are stimulating migration. For example, CXCR4 expressing melanoma, prostate or breast tumours may experience reduced metastasis with PKC and PKD inhibition [28,30]. However, CXCR5 expressing melanoma would only benefit from PKC inhibition. This highlights the necessity for identifying the tumour chemokine profile for the tailoring of personalised therapeutics.

4. Conclusion

As summarised in Fig. 7, we determined that PKC was involved in both CXCL12 and CXCL13 stimulated SK-MEL-28 migration however, PKD was only involved in CXCL12 and not CXCL13 stimulated SK-MEL-28 migration. Furthermore, PKC and PKD stimulate SK-MEL-28 cells to undergo actin cytoskeletal morphological changes during CXCL12 but not in CXCL13 stimulated SK-MEL-28 migration. Finally, both PKC and PKD were not involved in CXCL12 or CXCL13 stimulated THP-1 migration. This highlights that both PKC and PKD inhibitors could be valuable therapeutics for the prevention of CXCL12-induced metastatic melanoma but not for leukemic metastasis. However, the use of PKC inhibitors would be a broader therapeutic, preventing both CXCL12 and CXCL13 stimulated metastatic melanoma.

5. Materials and methods

5.1. Cell culture

Both the malignant melanoma SK-MEL-28 and the acute monocytic leukaemia THP-1 cell lines were obtained from ATCC (Teddington, UK).
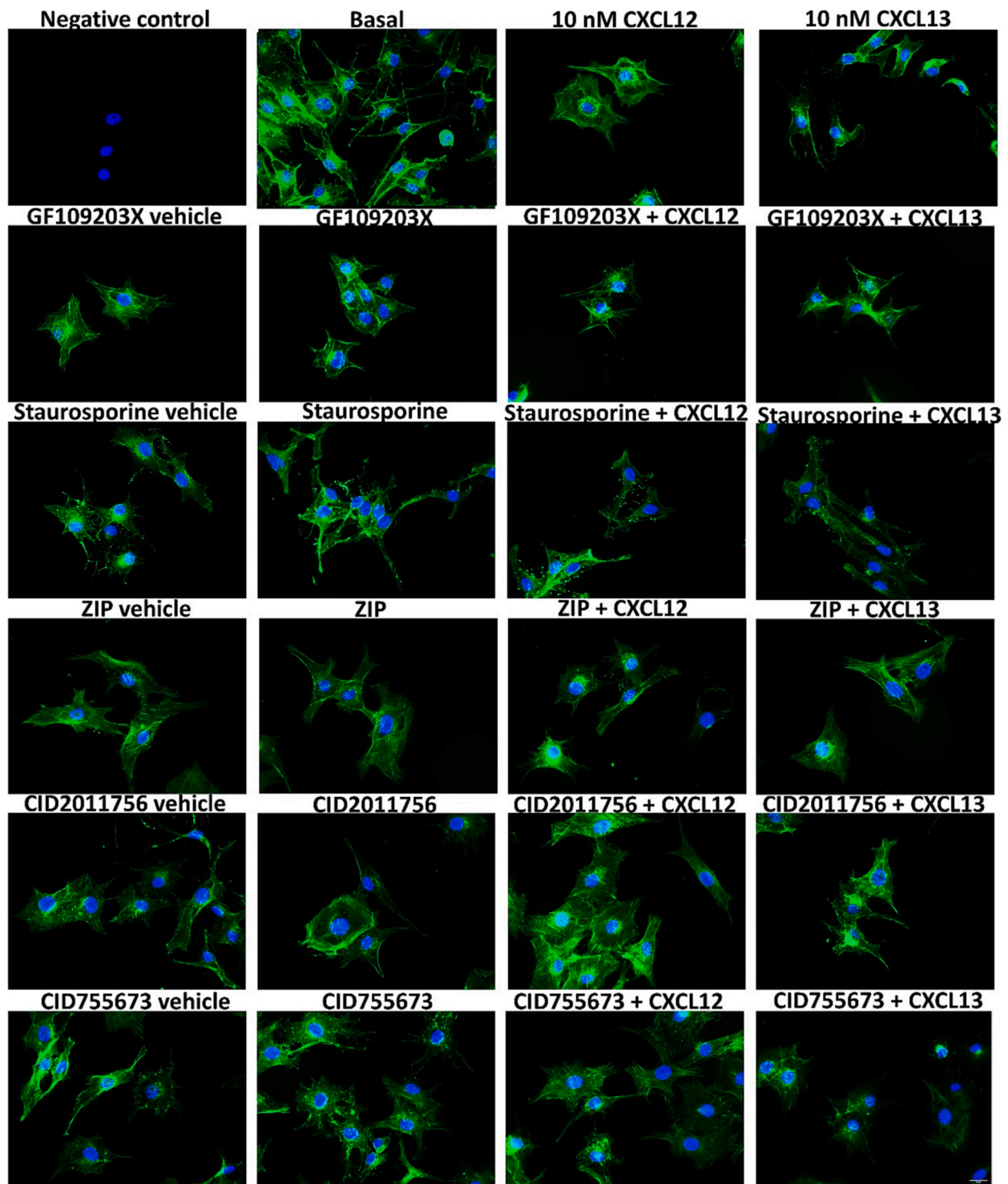
Fig. 4. PKC inhibitors decrease CXCL12 stimulated SK-MEL-28 cell shape changes. SK-MEL-28 cells were treated with 30 μM GF109203X, 100 nM staurosporine, 10 μM ZIP, 30 μM CID2011756 or 30 μM CID755673 ± 10 nM CXCL12 or 10 nM CXCL13 for 24 h. Actin cytoskeleton visualised using Phalloidin-iFluor 488 reagent (green) with nuclei indicated by DAPI staining (blue). Negative control visualised using DAPI staining only. Data shows representative cells from 4 independent experiments with similar findings. Acquired with Leica imaging suite, 40× objective (22× overall magnification). Scale bar is μm. Cell area and circularity calculated in Fig. 5. (For interpretation of the references to colour in this figure legend, the reader is referred to the web version of this article.)

Both cell lines were cultured in Rosewell Park Memorial Institute (RPMI) 1640 supplemented with 10% foetal calf serum, 1% non-essential amino acids and 1% L-glutamine. Cells were cultured at 37 °C in a 95%/5% air/ CO_2-humidified environment. THP-1 cells were sub-cultured when cell density reached 1×10^6 mL^{-1} and SK-MEL-28 cells were sub-cultured at 90% confluency by lifting with 1× versine (ThermoFisher Scientific,

Loughborough, UK). Both cell lines were not used beyond passage 30.

5.2. Materials

CXCL12 and CXCL13 were purchased from Peprotech (London, UK). Chemokines were made to a stock solution of 1 μM in H_2O. GF109203X
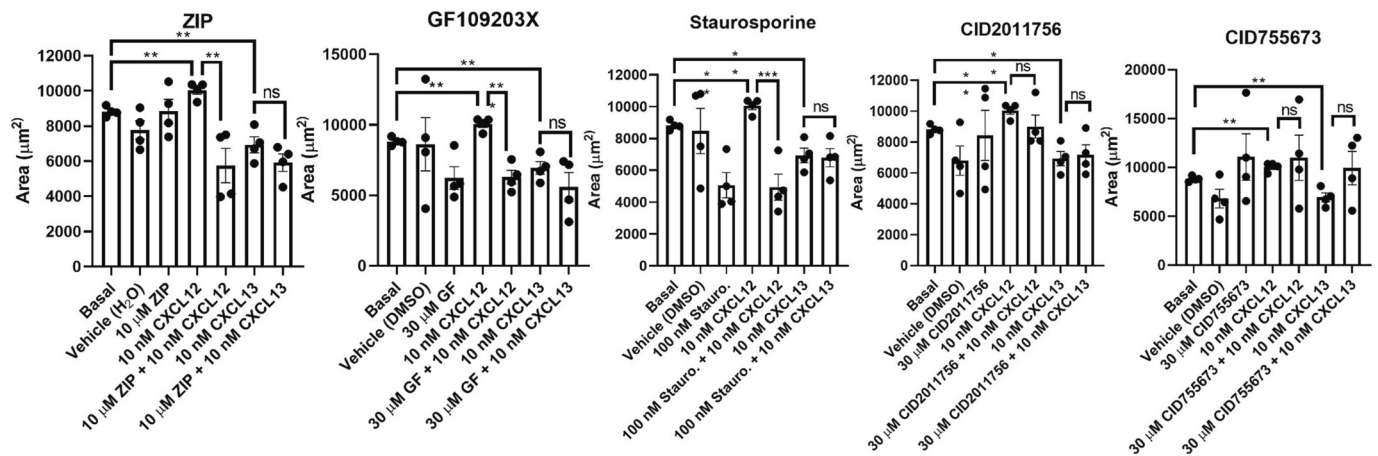
Fig. 5. PKC inhibitors decrease CXCL12 stimulated SK-MEL-28 cell surface area. SK-MEL-28 cells were treated with 30 μM GF109203X, 100 nM staurosporine, 10 μM ZIP, 30 μM CID2011756 or 30 μM CID755673 ± 10 nM CXCL12 or 10 nM CXCL13 for 24 h as depicted in Fig. 4. Cell area and circularity were measuring using ImageJ analysis software. 10 cells were measured per condition. Data are mean ± SEM, $N = 4$ analysed by two-tailed, unpaired t-tests. Ns not significant, $*p < 0.05$, $**p < 0.01$ and $***p < 0.001$.
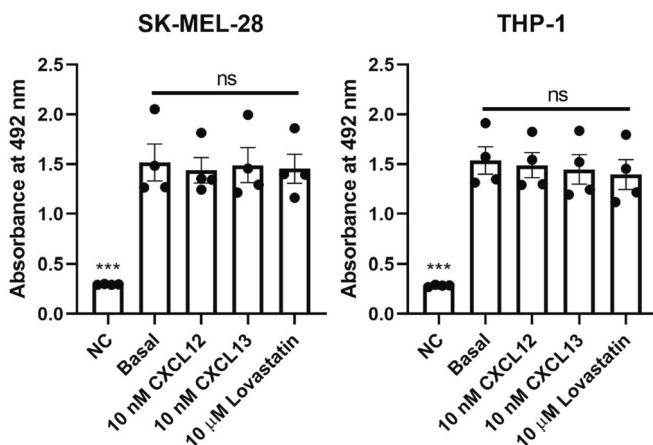

Fig. 6. CXCL12 and CXCL13 have no effect on SK-MEL-28 or THP-1 cell proliferation at concentrations used. SK-MEL-28 and THP-1 cells were treated with 10 nM CXCL12, 10 nM CXCL13 and 10 μM lovastatin for 72 h before treatment with 3-(4,5-dimethylthiazol-2-yl)-5-(3-carboxymethoxyphenyl)-2-(4-sulfophenyl)-2H-tetrazolium, inner salt; MTS for 1 h. Data are mean ± SEM, $N = 4$ analysed by two-tailed, unpaired t-tests. Ns not significant and $***p < 0.001$.

(stock solution of 23.5 mM in DMSO), CID2011756 (stock solution of 50 mM in DMSO), CID755673 (stock solution of 50 mM in DMSO) and lovastatin (stock solution 7 mM in DMSO) were purchased from Tocris (Abingdon, UK). Staurosporine (stock solution of 1 mM in DMSO) and PKCζ pseudo-substrate inhibitor, myristoylated also known as ZIP (stock solution of 1 mM in H_2O) were purchased from Santa Cruz Biotechnology (Heidelberg, Germany). Working concentrations were achieved by diluting chemokines and inhibitors in RPMI 1640 media. GF109203X is an α, βI, βII, γ, δ, ε and ζ PKC inhibitor with IC_{50} values of 8.4–20, 18, 16, 20, 210, 132 and 5800 nM, respectively [65,66]. ZIP is a PKCζ specific inhibitor with an IC_{50} value of 1–2.5 μM [67]). Staurosporine is an α, γ, η, δ, ε and ζ PKC inhibitor with and IC_{50} of 2, 5, 4, 20, 73 and 1086 nM, respectively [68]. CID2011756 is a PKD inhibitor with IC_{50} values of 0.6, 0.7 and 3.3 μM for PKD2, PKD3 and PKD1, respectively [51]. CID755673 is another PKD inhibitor with IC_{50} values of 0.182, 0.28, 0.23 and > 10 μM for PKD1, PKD2, PKD3 and PKC, respectively [29]. Lovastatin induces G1 cell cycle arrest in tumour cells lines thus inhibits proliferation [69,70].

5.3. Flow cytometry

Cells were harvested at a density of 1×10^6 mL^{-1} in 0.5% bovine serum albumin (BSA)/PBS. Cells were washed twice in ice-cold 1× PBS then incubated with primary mouse monoclonal anti-CXCR1 (IL-8RA, sc-7303, 1:50 dilution), anti-CXCR2 (IL-8RB, sc-7304, 1:50 dilution) anti-CXCR3 (sc-133,087, 1:200 dilution), anti-CXCR4 (12G5, 1:200 dilution) (Santa Cruz Biotechnology, Heidelberg, Germany), 1:50 anti-CXCR5 (MU5UBEE; Invitrogen, Inchinnan, UK), anti-CXCR6 (MAB2145, 1:50 dilution) or anti-CXCR7/ACKR3 (11G8, 1:50 dilution) (R&D Systems, Abingdon, UK) antibodies for 1 h at 4 °C. For negative control, no primary antibody was added. Cells were washed twice in ice-cold 1× PBS then incubated with 1:200 secondary goat anti-mouse Alexa Fluor® 488 (Abcam, Cambridge, UK) for 1 h at 4 °C. Cells were washed twice in ice-cold 1× PBS then analysed using a CytoFLEX (Beckman Coulter) with CytExpert (v2.4) software.

Data analysis: Median fluorescence was measured for each sample and relative fluorescence was calculated as sample/negative control then plotted using GraphPad Prism 8 software.

5.4. Immunofluorescence microscopy

SK-MEL-28 cells were seeded onto ethanol sterilised glass cover slides in a 12-well plate at a density of 0.5×10^5 mL^{-1} in RPMI 1640 media for 24 h at 37 °C in a 95%/5% air/CO$_2$-humidified environment. Cells were washed twice in ice-cold 1× PBS and fixed with 4% paraformaldehyde for 10 min. Cells were washed twice in ice-cold 1× PBS then incubated with 1:200 primary mouse anti-CXCR4 (12G5; Santa Cruz Biotechnology, Heidelberg, Germany) or 1:50 primary mouse anti-CXCR5 (MU5UBEE; Invitrogen, Inchinnan, UK) antibodies for 1 h at 4 °C. For negative control, no primary antibody was added. Cells were washed twice in ice-cold 1× PBS then incubated with 1:200 secondary goat anti-mouse Alexa Fluor® 488 (Abcam, Cambridge, UK) for 1 h at 4 °C. Cells were washed twice in ice-cold 1× PBS then incubated with DAPI (4′,6 diamidino-2-phenylindole; MERCK, Feltham, UK) for 10 min at 4 °C. Cells were washed twice in ice-cold 1× PBS and finally the cover slides were mounted onto glass slides using DPX mountant (Thermo-Fisher Scientific, Loughborough, UK). THP-1 cells were harvested, centrifuged then resuspended in ice-cold 1× PBS at a density of 2×10^6 mL^{-1} whereupon the above procedure was carried out with washing occurring by centrifugation and resuspension in 1× PBS. Finally, 10 μL of cell solution was pipetted into DPX mountant and a cover slide affix on top. Cells were visualised for CXCR4 and CXCR5 expression using a Leica DMIL LED inverted microscope using a 63× objective with an
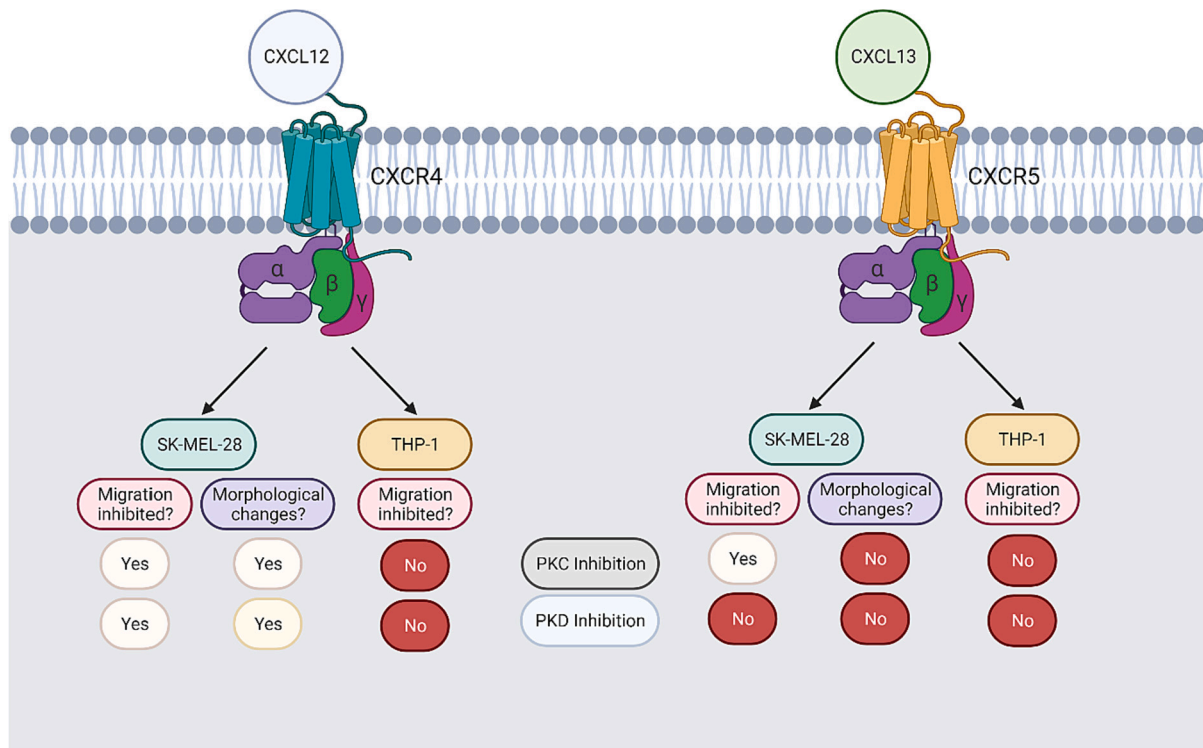
Fig. 7. Schematic representation of the effect of PKC and PKD inhibitors on CXCL12 and CXCL13 stimulated SK-MEL-28 and THP-1 cells.

overall magnification of 35×.

5.5. Time-lapse cell migration assay

The effect of selected PKC and PKD inhibitors upon CXCL12 and CXCL13 migration in SK-MEL-28 cells was observed using time-lapse microscopy. SK-MEL-28 cells were harvested at 0.4×10^4 mL^{-1} cells and seeded into 48-well plates in RPMI 1640 for 24 h at 37 °C in a 95%/5% air/CO$_2$-humidified environment. The following day cells were washed with 1× PBS and resuspended in serum-free RPMI 1640. Cells were challenged with 5 half log incremental concentrations of inhibitor within the tolerated toxicity range (GF109203X; 300 nM to 30 μM, staurosporine; 1 nM to 100 nM, ZIP; 300 nM to 10 μM, CID2011756; 300 nM to 30 μM and CID755673; 300 nM to 30 μM) in the presence and absence of 10 nM CXCL12 or 10 nM CXCL13, diluted in serum-free RPMI 1640. The 48 well plate was inserted into a controlled chamber at 37 °C in a 95%/5% air/CO$_2$-humidified environment. Time lapse images were taken using a 10× objective using a Zeiss Axio Observer 7 Inverted LED fluorescence motorised microscope with images captured every 5 min for 10 h (120 frames) using Zen-Lite v3–1 (Zeiss).

Data analysis: Using ImageJ software, any shift in the plate over time was corrected using Plugin, Registration, Linear stack alignment with SIFT. 10 cells per condition were manually tracked by clicking on the centre of the cell nuclei throughout consecutive frames. Average cell speed for each sample was calculated as migratory distance/time then averaged over 10 cells and plotted using GraphPad Prism 8 software. Exclusion criteria included cells that died, divided, or left the visual frame.

5.6. Chemotaxis assay

The effect of selected PKC and PKD inhibitors upon CXCL12 and CXCL13 migration in THP-1 cells was observed using ChemoTX 5 μM pore transwell chemotaxis plates (Neuroprobe Inc., Maryland, USA). Wells were blocked with 31 μL of serum free RPMI 1640 containing 1% BSA for 30 min at room temperature. Media was removed and replaced with 31 μL of 5 nM CXCL12 or 5 nM CXCL13 diluted in serum free RPMI 1640 containing 0.1% BSA. Serum free RPMI 1640 containing 0.1% BSA was used as a negative control. The 5 μM pore polyvinylprollidone-free polycarbonate membrane was then attached. THP-1 cells were harvested at a concentration of 50×10^4 mL^{-1} in serum free RPMI 1640 containing 0.1% BSA. Cells were challenged with 5 half log incremental concentrations of inhibitor within the tolerated toxicity range (GF109203X; 300 nM to 30 μM, staurosporine; 1 nM to 100 nM, ZIP; 100 nM to 10 μM, CID2011756; 300 nM to 30 μM and CID755673; 300 nM to 30 μM) and incubated for 30 min at 37 °C in a 95%/5% air/CO$_2$-humidified environment. Cells were washed and resuspended in serum free RPMI 1640 containing 0.1% BSA and 20 μL of cells were loaded onto the surface of the 5 μM pore membrane. The plate was placed inside a humidified chamber and incubated for 4 h at 37 °C in a 95%/5% air/CO$_2$-humidified environment. The filter was then removed, and 10 μL of cells were counted from each lower chamber using a haemocytometer to determine the number of cells that had migrated towards the chemokine.

Data analysis: Duplicates of each condition were carried out. The number of migrating cells per condition was counted then averaged and plotted using GraphPad Prism 8 software.

5.7. Actin staining and cell morphology analysis

SK-MEL-28 cells were harvested and 1×10^5 mL^{-1} cells were seeded in RPMI 1640 onto ethanol sterilised glass cover slides in a 12-well plate. Maximum tolerated concentrations of each inhibitor were added to the plate (30 μM GF109203X, 100 nM staurosporine, 10 μM ZIP, 30 μM CID2011756 and 30 μM CID755673) with and without 10 nM CXCL12 or CXCL13 and left to incubate for 24 h at 37 °C in a 95%/5% air/CO$_2$-humidified environment. Cells were washed twice with 1× PBS then fixed with 4% paraformaldehyde for 10 min at room temperature. Cells were washed twice with 1× PBS then permeabilized with 0.1% Triton X-100 for 5 min. Cells were washed twice with 1× PBS then incubated with 1:1000 Phalloidin-iFluor 488 reagent (Abcam, Cambridge, UK) suspended in 1% BSA/PBS for 30 min. Cells were washed twice in 1× PBS

and 1:1000 DAPI in $1\times$ PBS was added for 10 min. Cells were washed twice with $1\times$ PBS and finally the cover slides were mounted onto glass slides using DPX mountant. Cells were visualised using a Leica DMIL LED inverted microscope using a $40\times$ objective with an overall magnification of $22\times$.

Data analysis: Using ImageJ software, the polygon tool was used to manually draw around 10 cells per condition. Cell area and circularity were analysed using Analyse, Set measurements, area, and shape descriptors. Average cell area was plotted in GraphPad Prism 8 software. Exclusion criteria included cells where the whole area could not be measured and cells that were in the process of dividing.

5.8. Cell viability assay

CellTiter 96® AQ$_{ueous}$ One Solution Cell Proliferation Assay (Promega, Southampton, UK) containing a tetrazolium compound [3-(4,5-dimethylthiazol-2-yl)-5-(3-carboxymethoxyphenyl)-2-(4-sulfophenyl)-2H-tetrazolium, inner salt; MTS] was used to determine cell viability. 100 µL of cells were seeded at 1×10^5 mL^{-1} into clear 96-well plates. Cells were challenged with half log incremental concentrations of inhibitor (GF109203X; 300 nM to 30 µM, staurosporine; 1 nM to 1000 nM, ZIP; 100 nM to 30 µM, CID2011756; 300 nM to 30 µM and CID755673; 300 nM to 30 µM) or 10 nM chemokine and 10 µM lovastatin and incubated for 72 h at 37 °C in a 95%/5% air/CO$_2$-humidified environment. 10 µL of MTS reagent was added to each well and incubated for 4 h at 37 °C in a 95%/5% air/CO$_2$ humidified environment. A FLUOstar Optima Fluorometer using Optima software (BMG Labtech) was used at an absorbance of 490 nm to detect the quantity of the coloured formazan product.

Data analysis: Triplicates of each condition were carried out. Percentage survival was calculated as; (average absorbance of sample/ average absorbance of positive control) x 100 and plotted using GraphPad Prism 8 software.

5.9. Statistical analysis

Experiments were repeated on cells where N represents the number of biological repeats $\pm$ the Standard Error of the Mean (SEM). For Tables 1, 3 and 4 and Figs. 1, 3 and 4 data were analysed by one-way ANOVA with post hoc Dunnett's multiple comparison test. Data calculated as $p < 0.05$ was considered statistically significant and is graphically represented as ****$p < 0.0001$, ***$p < 0.001$, **$p < 0.01$ and *$p < 0.05$. IC$_{50}$ and pIC$_{50}$ values displayed in Fig. 2 and Table 3 were determined by using Log (Inhibitor) vs. response–Variable slope (four parameters) with the Hill Slope set to 1 using GraphPad Prism 8 software. For Figs. 3, 5 and 6, data were analysed by two-tailed unpaired *t*-test. Data calculated as $p < 0.05$ was considered statistically significant and is graphically represented as ****$p < 0.0001$, ***$p < 0.001$, **$p < 0.01$ and *$p < 0.05$.

Credit author statement

I·H co-conceptualized, curated, and analysed data, conducted investigation, contributed methodology, managed the project, handled visualisation, wrote both original draft and reviewed and edited the manuscript. Y.E, A.M, L.N and D.O.J curated and analysed data. A. Mueller co-conceptualized the project and edited the manuscript.

Funding

Declaration of Competing Interest

The authors declare that there is no conflict of interest.

Data availability

Data will be made available on request.

References

[1] H. Dillekås, M.S. Rogers, O. Straume, Are 90% of deaths from cancer caused by metastases? Cancer Med. 8 (12) (2019) 5574–5576.

[2] C.L. Chaffer, R.A. Weinberg, A perspective on cancer cell metastasis, Science 331 (6024) (2011) 1559–1564.

[3] S. Paget, The distribution of secondary growths in cancer of the breast, Lancet 133 (3421) (1889) 571–573.

[4] P.J. Sarvaiya, et al., Chemokines in tumor progression and metastasis, Oncotarget 4 (12) (2013) 2171.

[5] M. O'Hayre, et al., Chemokines and cancer: migration, intracellular signalling and intercellular communication in the microenvironment, Biochem. J. 409 (3) (2008) 635–649.

[6] J.W. Griffith, C.L. Sokol, A.D. Luster, Chemokines and chemokine receptors: positioning cells for host defense and immunity, Annu. Rev. Immunol. 32 (2014) 659–702.

[7] W.Y. Lai, A. Mueller, Latest update on chemokine receptors as therapeutic targets, Biochem. Soc. Trans. 49 (3) (2021) 1385–1395.

[8] C. Larsson, Protein kinase C and the regulation of the actin cytoskeleton, Cell. Signal. 18 (3) (2006) 276–284.

[9] A.C. Newton, Protein kinase C: poised to signal, Am. J. Physiol. Endocrinol. Metab. 298 (2010) E395–402.

[10] M. Hussain, et al., CXCL13/CXCR5 signaling axis in cancer, Life Sci. 227 (2019) 175–186.

[11] Y. Shi, D.J. Riese, J. Shen, The role of the CXCL12/CXCR4/CXCR7 chemokine axis in cancer, Front. Pharmacol. 11 (2020), 574667.

[12] C. Keenan, A. Long, D. Kelleher, Protein kinase C and T cell function, Biochim. Biophys. Acta (BBA)-Mol. Cell Res. 1358 (2) (1997) 113–126.

[13] E.A. Nalefski, J.J. Falke, The C2 domain calcium-binding motif: structural and functional diversity, Protein Sci. 5 (12) (1996) 2375–2390.

[14] M. Montiel, E.P. de la Blanca, E. Jiménez, P2Y receptors activate MAPK/ERK through a pathway involving PI3K/PDK1/PKC-ζ in human vein endothelial cells, Cell. Physiol. Biochem. 18 (1–3) (2006) 123–134.

[15] K. Kolczynska, et al., Diacylglycerol-evoked activation of PKC and PKD isoforms in regulation of glucose and lipid metabolism: a review, Lipids Health Dis. 19 (2020) 1–15.

[16] M. Cobbaut, et al., Differential regulation of PKD isoforms in oxidative stress conditions through phosphorylation of a conserved Tyr in the P+ 1 loop, Sci. Rep. 7 (1) (2017) 1–17.

[17] K. Zhang, et al., PKD1 inhibits cancer cells migration and invasion via Wnt signaling pathway in vitro, Cell Biochem. Funct. Cell. Biochem. Modul. Active Agents Dis. 25 (6) (2007) 767–774.

[18] T. Eiseler, et al., PKD is recruited to sites of actin remodelling at the leading edge and negatively regulates cell migration, FEBS Lett. 581 (22) (2007) 4279–4287.

[19] A. Alpsoy, U. Gündüz, Protein kinase D2 silencing reduced motility of doxorubicin-resistant MCF7 cells, Tumor Biol. 36 (2015) 4417–4426.

[20] P. Peterburs, et al., Protein kinase D regulates cell migration by direct phosphorylation of the cofilin phosphatase slingshot 1 like, Cancer Res. 69 (14) (2009) 5634–5638.

[21] S. Kumari, et al., Protein kinase D1 regulates metabolic switch in pancreatic cancer via modulation of mTORC1, Br. J. Cancer 122 (1) (2020) 121–131.

[22] C.M. Dowling, et al., Expression of protein kinase C gamma promotes cell migration in colon cancer, Oncotarget 8 (42) (2017) 72096.

[23] T.N. Pham, et al., Protein kinase C α enhances migration of breast cancer cells through FOXC2-mediated repression of p120-catenin, BMC Cancer 17 (1) (2017) 1–13.

[24] X. Yuan, et al., Inhibition of protein kinase C by isojacareubin suppresses hepatocellular carcinoma metastasis and induces apoptosis in vitro and in vivo, Sci. Rep. 5 (1) (2015) 12889.

[25] M. Tallman, et al., Acute monocytic leukemia (French-American-British classification M5) does not have a worse prognosis than other subtypes of acute myeloid leukemia: a report from the Eastern Cooperative Oncology Group, J. Clin. Oncol. Off. J. Am. Soc. Clin. Oncol. 22 (7) (2004) 1276–1286.

[26] S. Tsuchiya, et al., Establishment and characterization of a human acute monocytic leukemia cell line (THP-1), Int. J. Cancer 26 (2) (1980) 171–176.

[27] E. Alassaf, A. Mueller, The role of PKC in CXCL8 and CXCL10 directed prostate, breast and leukemic cancer cell migration, Eur. J. Pharmacol. 886 (2020), 173453.

[28] I. Hamshaw, M. Ajdarirad, A. Mueller, The role of PKC and PKD in CXCL12 directed prostate cancer migration, Biochem. Biophys. Res. Commun. 519 (1) (2019) 86–92.

[29] E.R. Sharlow, et al., Potent and selective disruption of protein kinase D functionality by a benzoxoloazepinolone, J. Biol. Chem. 283 (48) (2008) 33516–33526.

[30] S.C. Mills, et al., Cell migration towards CXCL12 in leukemic cells compared to breast cancer cells, Cell. Signal. 28 (4) (2016) 316–324.

[31] A.E. Vilgelm, A. Richmond, Chemokines modulate immune surveillance in tumorigenesis, metastasis, and response to immunotherapy, Front. Immunol. 10 (2019) 333.

[32] W.E. Damsky Jr., L.E. Rosenbaum, M. Bosenberg, Decoding melanoma metastasis, Cancers 3 (1) (2010) 126–163.

[33] A.E. Whiteley, et al., Leukaemia: a model metastatic disease, Nat. Rev. Cancer 21 (7) (2021) 461–475.

[34] K. Mortezaee, CXCL12/CXCR4 axis in the microenvironment of solid tumors: a critical mediator of metastasis, Life Sci. 249 (2020), 117534.

[35] E.M. García-Cuesta, et al., The role of the CXCL12/CXCR4/ACKR3 axis in autoimmune diseases, Front. Endocrinol. 10 (2019) 585.

[36] T. Koshiba, et al., Expression of stromal cell-derived factor 1 and CXCR4 ligand receptor system in pancreatic cancer: a possible role for tumor progression, Clin. Cancer Res. 6 (9) (2000) 3530–3535.

[37] A. Müller, et al., Involvement of chemokine receptors in breast cancer metastasis, Nature 410 (6824) (2001) 50–56.

[38] S. Singh, et al., CXCL12–CXCR4 interactions modulate prostate cancer cell migration, metalloproteinase expression and invasion, Lab. Investig. 84 (12) (2004) 1666–1676.

[39] S.-B. Peng, et al., Identification of LY2510924, a novel cyclic peptide CXCR4 antagonist that exhibits antitumor activities in solid tumor and breast cancer metastatic models, Mol. Cancer Ther. 14 (2) (2015) 480–490.

[40] Y. Gao, et al., CXCR4 as a novel predictive biomarker for metastasis and poor prognosis in colorectal cancer, Tumor Biol. 35 (2014) 4171–4175.

[41] S. Otsuka, et al., CXCR4 overexpression is associated with poor outcome in females diagnosed with stage IV non-small cell lung cancer, J. Thorac. Oncol. 6 (7) (2011) 1169–1178.

[42] A. Peled, et al., Role of CXCL12 and CXCR4 in the pathogenesis of hematological malignancies, Cytokine 109 (2018) 11–16.

[43] A. McConnell, et al., The prognostic significance and impact of the CXCR4–CXCR7–CXCL12 axis in primary cutaneous melanoma, Br. J. Dermatol. 175 (6) (2016) 1210–1220.

[44] R.M. Kotb, et al., Potential role of CXCR4 in trastuzumab resistance in breast cancer patients, Biochim. Biophys. Acta (BBA)-Mol. Basis Dis. 1868 (11) (2022), 166520.

[45] C.C. Chao, et al., CXC chemokine ligand-13 promotes metastasis via CXCR5-dependent signaling pathway in non-small cell lung cancer, J. Cell. Mol. Med. 25 (19) (2021) 9128–9140.

[46] J. Meijer, et al., The CXCR5 chemokine receptor is expressed by carcinoma cells and promotes growth of colon carcinoma in the liver, Cancer Res. 66 (19) (2006) 9576–9582.

[47] A. Bürkle, et al., Overexpression of the CXCR5 chemokine receptor, and its ligand, CXCL13 in B-cell chronic lymphocytic leukemia, Blood 110 (9) (2007) 3316–3325.

[48] L. Jiang, et al., CXCL13/CXCR5 are potential biomarkers for diagnosis and prognosis for breast cancer, Age (years) 31 (56) (2020) 70.

[49] S. Singh, et al., Clinical and biological significance of CXCR5 expressed by prostate cancer specimens and cell lines, Int. J. Cancer 125 (10) (2009) 2288–2295.

[50] C.M. Cardaba, et al., CCL3 induced migration occurs independently of intracellular calcium release, Biochem. Biophys. Res. Commun. 418 (1) (2012) 17–21.

[51] E.R. Sharlow, et al., Discovery of diverse small molecule chemotypes with cell-based PKD1 inhibitory activity, PLoS One 6 (10) (2011), e25134.

[52] H. Yamaguchi, J. Condeelis, Regulation of the actin cytoskeleton in cancer cell migration and invasion, Biochim. Biophys. Acta (BBA)-Mol. Cell Res. 1773 (5) (2007) 642–652.

[53] B.S. Fogh, H.A. Multhaupt, J.R. Couchman, Protein kinase C, focal adhesions and the regulation of cell migration, J. Histochem. Cytochem. 62 (3) (2014) 172–184.

[54] H. Stensman, C. Larsson, Protein kinase Cepsilon is important for migration of neuroblastoma cells, BMC Cancer 8 (2008) 1–13.

[55] B. Huck, et al., GIT1 phosphorylation on serine 46 by PKD3 regulates paxillin trafficking and cellular protrusive activity, J. Biol. Chem. 287 (41) (2012) 34604–34613.

[56] A. Woods, J.R. Couchman, Protein kinase C involvement in focal adhesion formation, J. Cell Sci. 101 (2) (1992) 277–290.

[57] D.-S. Chae, et al., Priming stem cells with protein kinase C activator enhances early stem cell-chondrocyte interaction by increasing adhesion molecules, Biol. Res. 51 (2018).

[58] H.R. Döppler, et al., Protein kinase D1-mediated phosphorylations regulate vasodilator-stimulated phosphoprotein (VASP) localization and cell migration, J. Biol. Chem. 288 (34) (2013) 24382–24393.

[59] N. Durand, et al., Protein kinase D1 regulates focal adhesion dynamics and cell adhesion through Phosphatidylinositol-4-phosphate 5-kinase type-l γ, Sci. Rep. 6 (1) (2016) 35963.

[60] S.R. Gabbireddy, et al., Melanoma cells adopt features of both mesenchymal and amoeboid migration within confining channels, Sci. Rep. 11 (1) (2021) 17804.

[61] M. Bergert, et al., Cell mechanics control rapid transitions between blebs and lamellipodia during migration, Proc. Natl. Acad. Sci. 109 (36) (2012) 14434–14439.

[62] T. Lämmermann, et al., Rapid leukocyte migration by integrin-independent flowing and squeezing, Nature 453 (7191) (2008) 51–55.

[63] J. Renkawitz, et al., Adaptive force transmission in amoeboid cell migration, Nat. Cell Biol. 11 (12) (2009) 1438–1443.

[64] M. Morimatsu, et al., Migration arrest of chemoresistant leukemia cells mediated by MRTF-SRF pathway, Inflamm. Regenerat. 40 (1) (2020) 1–9.

[65] D. Toullec, et al., The bisindolylmaleimide GF 109203X is a potent and selective inhibitor of protein kinase C, J. Biol. Chem. 266 (24) (1991) 15771–15781.

[66] G. Martiny-Baron, et al., Selective inhibition of protein kinase C isozymes by the indolocarbazole Gö 6976, J. Biol. Chem. 268 (13) (1993) 9194–9197.

[67] P. Serrano, Y. Yao, T.C. Sacktor, Persistent phosphorylation by protein kinase Mζ maintains late-phase long-term potentiation, J. Neurosci. 25 (8) (2005) 1979–1984.

[68] T. Tamaoki, et al., Staurosporine, a potent inhibitor of phospholipidCa++ dependent protein kinase, Biochem. Biophys. Res. Commun. 135 (2) (1986) 397–402.

[69] K. Asakura, et al., The cytostatic effects of lovastatin on ACC-MESO-1 cells, J. Surg. Res. 170 (2) (2011) e197–e209.

[70] W. Park, et al., Lovastatin-induced inhibition of HL-60 cell proliferation via cell cycle arrest and apoptosis, Anticancer Res. 19 (4B) (1999) 3133–3140.